PAPER

Check for updates

Cetyltrimethylammonium chloride-loaded mesoporous silica nanoparticles as a mitochondrion-targeting agent for tumor therapy†

Menghuan Tang,[a] Peng Zhang,[b] Jiahui Liu,[a] Yijuan Long, [ID][a] Yuan Cheng*[b] and Huzhi Zheng [ID]*[a]

Mitochondria play an important role in supplying cellular energy, cell signaling and governing cell death. In addition, mitochondria have also been proved to be essential for tumor generation and development. Thus, mitochondrion-targeting therapeutics and treatments have emerged as promising strategies against cancer. However, the lack of mitochondrion-targeting agents has limited their application. To this end, we report cetyltrimethylammonium chloride-loaded mesoporous silica nanoparticles conjugated with human serum albumin (CTAC@MSNs-HSA) as a mitochondrion-targeting agent for anticancer treatment. As the structure-directing agent in the synthesis of MSNs, CTAC is stored within MSNs. Due to their desirable size and HSA receptor-mediated transcytosis, CTAC@MSNs-HSA show great cellular uptake and enhanced accumulation in the cytoplasm. Positively charged CTAC could actively target mitochondria by interacting with the negatively charged mitochondria membrane, and then lead to the dysfunction of mitochondria by decreasing mitochondrial potential and intracellular ATP levels, resulting in the necrosis and apoptosis of MCF-7 cells. Therefore, significant antitumor activity is observed by *in vitro* studies. Moreover, *in vivo* studies confirm that the CTAC@MSNs-HSA are able to induce cancer cell death and efficiently inhibit tumor growth. These results demonstrate the potential of CTAC@MSNs-HSA in cancer therapeutics as well as providing insights into mitochondrion-targeting treatment.

1. Introduction

Mitochondrion is a common membrane-coated organelle that participates in energy conversion, homeostasis of calcium, cell signaling and cell death.[1] It has become increasingly evident that mitochondria play a key role in the generation, proliferation and metastasis of cancer cells.[2] Mitochondria of cancer cells are different from those of normal cells in many ways.[3] For instance, mtDNA mutations and mitochondrial dysfunction have been observed in various types of cancer.[4] The mitochondrial membrane potential of cancer cells (~ -220 mV) is more negative than that of normal cells (~ -160 mV).[5] Therefore, mitochondria have been regarded as a novel target for cancer therapy.[6] Numerous research studies have been carried out to construct mitochondrion-targeted therapeutics.[7,8] Chloroquine, an United States Food and Drug Administration-approved

inhibitor of autophagy, has been revealed to possess antitumor property for impairing mitochondrial metabolism. It has also been shown that metformin and phenformin inhibit tumor growth by disrupting mitochondrial complex.[9] Although the design of nanoparticles with triphenylphosphonium cation (TPP, the mitochondrion-targeting moiety) offers potential for mitochondrion-targeting therapeutics, it is still a challenge to actively deliver therapeutic agents to mitochondria due to the selective permeability of the mitochondrial membrane.[3,5]
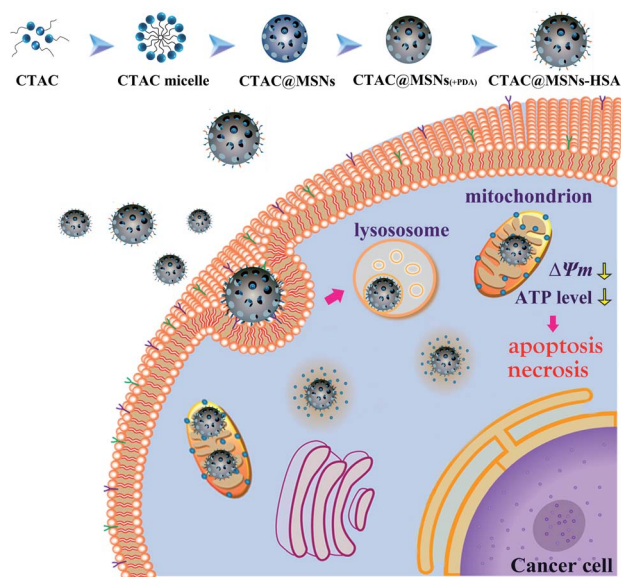
Some surfactants, such as cetyltrimethylammonium bromide (CTAB), Tween 80, F127 and sodium dodecyl benzene sulfonate (SDBS) were reported as chemosensitizers to overcome the multidrug resistance (MDR) in cancer.[10–12] Noticeably, cationic surfactant is more extensively used in tumor treatment than other types of surfactants, such as anionic and nonionic surfactant.[13] CTAB and its derivatives are common components of the broad-spectrum antiseptics. CTAB has been shown as a promising compound against head and neck cancer cells with minimal toxicity against normal fibroblasts, as well as a tumoricidal irritant in colorectal cancer surgery.[14] However, previous reports on the antitumor activity of cationic surfactant have not been investigated thoroughly. On the other hand, due to lack of specificity, cationic surfactant may cause certain side

[a]Key Laboratory of Luminescent and Real-Time Analytical Chemistry (Southwest University), Ministry of Education, College of Chemistry and Chemical Engineering, Southwest University, Chongqing, 400715, P. R. China. E-mail: zhenghz@swu.edu.cn

[b]Department of Neurosurgery, The Second Affiliated Hospital of Chongqing Medical University, Chongqing, 400010, P. R. China

† Electronic supplementary information (ESI) available: Photographic images, zeta potential, and cytotoxicity assays. See DOI: 10.1039/d0ra02023k

Scheme 1 Synthesis of CTAC@MSNs-HSA and the mitochondrion-targeting therapy.

effects, which affect its antitumor activity and application in cancer therapy.

Nanomaterials have received considerable interest as efficient drug carriers for cancer therapy owing to its unique features.[10,15–19] In particular, mesoporous silica nanoparticles (MSNs) possess uniform and tunable size, high surface area, facile surface functionalization, biocompatibility, all of which make MSNs popular nanocarriers in drug delivery system.[20–22] MSNs are usually prepared using cationic surfactants as the sacrificial template. Inspired by the biological application of cationic surfactant, we use cetyltrimethylammonium chloride (CTAC), a cheap cationic surfactant, both as a template to prepare MSNs and an anticancer agent. As shown in Scheme 1, CTAC@MSNs were conjugated with human serum albumin (HSA), which enables the nanoparticle to actively target tumor cells *via* gp60 and SPARC receptor-mediated transcytosis while maintaining great biocompatibility.[23] Owing to the more negatively charged mitochondrial membrane of cancer cells, CTAC can actively target the mitochondria of cancer cells and cause mitochondrial damage. It shows remarkable antitumor efficacy against MCF-7 cells *in vitro* and regresses tumors on mouse models. Furthermore, CTAC@MSNs-HSA display high antitumor efficacy against MCF-7/ADR cells.[24]

2. Experimental section

2.1 Materials

Cetyltrimethylammonium chloride (CTAC), folic acid (FA), 3-aminopropyltriethoxysilane (APTES), tetraethyl orthosilicate (TEOS), dopamine hydrochloride, triethanolamine (TEA) and N,N-dimethylformamide (DMF) were purchased from Aladdin Reagent (Shanghai, China). Human serum albumin (HSA) was supplied by Biosynthesis Biotechnology Co. Ltd (Beijing,

China). The cell counting kit-8 (CCK-8) was acquired from Dojindo Laboratories (Kumamoto, Japan). Caspase-3 activity assay kit, lactate dehydrogenase (LDH) cytotoxicity assay kit, adenosine triphosphate (ATP) assay kit, 4′,6-diamidino-2-phenylindole (DAPI), Hoechst staining kit, TdT-mediated dUTP Nick-End Labeling (TUNEL) apoptosis assay kit and mitochondrial membrane potential assay kit (JC-1) were purchased from Beyotime Institute of Biotechnology (Shanghai, China). LysoTracker Green was purchased from Yeasen Biotech Co. Ltd (Shanghai, China). MitoLite Blue was purchased from AAT Bioquest Inc. (CA, USA). Alexa Fluor 488-dextran (10 000 MW) was purchased from Thermo Fisher Scientific Inc. (MA, USA). All other reagents were of analytical grade. Ultrapure water (18.2 MΩ) was prepared with a Milli-Q water purification system (Merck Millipore, USA) and used in all experiments.

2.2 Synthesis of NPs

2.2.1 Synthesis of MSNs, CTAC@MSNs, CTAC@MSNs-TRITC. CTAC@MSNs were prepared according to the micelle-template method with minor modifications.[24] CTAC (2.0 g), H_2O (20 mL), and triethanolamine (TEA, 0.02 g) were mixed and stirred at 95 °C for 1 h. Thereafter, 1.5 mL TEOS was added into the mixture drop-wise under constant stirring. After stirring for 1 h, the reaction solution was cooled to room temperature and the resultant was separated by centrifugation (8000 rpm, 10 min). After washed three times with ethanol, the obtained CTAC@MSNs were dried in a vacuum at 55 °C overnight. To obtain MSNs, CTAC@MSNs were calcinated at 650 °C for 6 h to remove surfactant molecules.[21] CTAC@MSNs were labeled with tetramethylrhodamine-6-isothiocyanate (TRITC) to track the cellular uptake of CTAC@MSNs.[25] First, 20 mg CTAC@MSNs were dispersed in DMF. Then 100 μL APTES was added and the mixture solution was stirred overnight. The product was collected by centrifugation (8000 rpm, 10 min) and washed with ethanol several times. Then 5 mg TRITC was added and reacted with CTAC@MSNs-NH_2 in the dark for 12 h. CTAC@MSNs-TRITC were obtained by centrifugation (8000 rpm, 10 min) and washed with ultrapure water several times, then dried under vacuum at room temperature.

2.2.2 Synthesis of CTAC@MSNs-HSA. 60 mg CTAC@MSNs were dispersed in phosphate buffer saline (PBS, 25 mL, 50 mM, pH = 8.5). Then, 12.5 mg of dopamine hydrochloride was added into the mixture, which was incubated in the dark with gentle stirring for 6 h. The product was collected by centrifugation (8000 rpm, 10 min) and washed with ultrapure water three times. Immediately after the polydopamine (PDA) coating, 50 mg HSA was solubilized in PBS (25 mL, 50 mM, pH = 8.5) and the solution was added into the above resultant followed by stirring for 12 h in the dark. HSA coated nanoparticles were obtained by centrifugation and washed with ultrapure water three times, then, dispersed in 25 mL PBS (50 mM, pH 8.5). To block the excessive sites of PDA surfaces, 50 mg of FA were mixed with the solution and the mixture was stirring for 12 h in the dark. The resultant product was centrifuged (8000 rpm, 10 min) and washed with ultrapure water three times.

2.3 Characterizations of nanoparticles (NPs)

To investigate the morphology, the samples were analysed by JEM-1200EX (JEOL Technics, Tokyo, Japan) transmission electron microscope (TEM). The hydrodynamic diameters and zeta potential of the nanoparticles were measured by Zetasizer Nano-ZS90 (Malvern, UK). Thermogravimetric analysis was conducted by SDT Q600 (TA, USA). Fourier transform infrared spectra (FT-IR) of the samples were collected with iS10 FT-IR spectrometer (Nicolet, USA).

2.4 *In vitro* antitumor activity studies

To investigate the antitumor activities of MSNs, CTAC@MSNs and CTAC@MSNs-HSA, their cytotoxicity against human breast cancer cells (MCF-7), multidrug resistant human mammary adenocarcinoma cells (MCF-7/ADR), mouse breast cancer cells (4T1), mouse glioma cells (C6) and human normal mammary epithelial cells (MCF-10A) were assayed by CCK-8 method. Briefly, cells were seeded into 96-well plates at 5×10^3 cells per well in 100 μL of medium and incubated at 37 °C overnight. Then, cells were treated with MSNs, CTAC@MSNs and CTAC@MSNs-HSA at various CTAC concentrations (0–50 μg mL^{-1}) for 24 h or 48 h. At the end of incubation, the culture medium was removed and cells were washed with PBS. The cell viabilities were then evaluated using the CCK-8 assay according to the standard protocol suggested by the manufacturer.

2.5 LDH release assay and Hoechst staining

In brief, the MCF-7 cells were seeded into 96-well plates at a density of 8×10^3 cells per well and incubated overnight. The cells were then washed with PBS and the culture medium was replaced by serum-free medium containing MSNs or CTAC@MSNs at a CTAC concentration of 2 μg mL^{-1}. Then lactate dehydrogenase (LDH) release levels were determined using LDH activity assay kit as instructed by the manufacturer.

MCF-7 cells (1×10^5 cells) were seeded in 35 mm glass-bottom culture dishes and allowed to attach for 24 h. Then cells were incubated with 2 μg mL^{-1} CTAC@MSNs-TRITC for 6 h. After that, the cells were washed with PBS and stained with Hoechst 33 258 for 30 min. Subsequently, cells were washed with PBS and followed by fixing with 4% paraformaldehyde for 10 min. Fluorescence imaging was performed on a U-TVO.5XC-2 fluorescence microscopy (Olympus, Japan).

2.6 Cellular colocalization imaging

MCF-7 cells (5×10^5 cells) were seeded into 35 mm glass-bottom culture dishes and incubated overnight. Then cells were incubated with 2 μg mL^{-1} CTAC@MSNs-TRITC for 2 and 6 h. After that, cells were washed with washed with PBS and stained with MitoLite Blue (mitochondrion dye) and Lyso-Tracker Green (lysosome dye) for 1 h. Then cells were washed with PBS and visualized under Confocal Laser Scanning Microscopy (CLSM) (Leica TCS SP8, Germany) with 60× oil-immersion objective. MitoLite Blue, LysoTracker Green and CTAC@MSNs-TRITC were excited at the wavelength of 405, 405, and 552 nm to emit blue, green and red luminescence,

respectively. There was no interference in the emission wavelengths that ranged from 480 to 500 nm for MitoLite Blue 500–530 nm for LysoTracker Green and 560–590 nm for CTAC@MSNs-TRITC.

2.7 Mitochondrial membrane potential and ATP level

The mitochondrial membrane potential ($\Delta \Psi_m$) was detected using JC-1. The MCF-7 cells were seeded into 24-well plates at a density of 1×10^5 cells per well and incubated overnight. The culture medium was removed and cells were cultured with MSNs, CTAC@MSNs for 24 h, then the cells were incubated with JC-1 staining solution for 20 min and rinsed three times with staining buffer. The green fluorescent intensity at 530 nm (excited with 485 nm) and red fluorescent intensity at 590 nm (excited with 530 nm) were detected by a microplate reader (Infinite M200 Pro, Tecan, Austria), respectively.

To measure the ATP level, MCF-7 cells were seeded into 24-well plates (1×10^5 cells per well) and allowed to attach for 24 h. The media was replaced with fresh medium containing 20 μg mL^{-1} MSNs, CTAC and CTAC@MSNs and incubation for 24 h. Then intracellular ATP levels were measured using the luciferin-luciferase-based ATP luminescence assay and instructed by the specification.

2.8 Visualization of lysosomal membrane permeabilization (LMP) and assay of caspase-3 activity

The cells were seeded in 15 mm glass bottomed culture dishes (1×10^4 cells per dish). And cells were incubated with 100 μg mL^{-1} Alexa Fluor 488 dextran for 1 h and then the culture media were replaced by fresh medium containing MSNs and CTAC@MSNs. After another 4 h culture, fluorescence images were obtained by an inverted fluorescence microscope (IX70, Olympus) equipped with a 100× oil-immersion objective (NA = 1.30).

Caspase-3 activity was measured by caspase-3 activity assay kit. The MCF-7 cells were seeded into 6-well plates (1×10^5 cells per well) and incubated overnight. Then the culture medium was replaced by fresh culture medium containing MSNs (20 μg mL^{-1}) and CTAC@MSNs at a CTAC concentration of 2 μg mL^{-1}. After incubation for 24 h, caspase-3 activity was determined at 405 nm using microplate reader (Infinite M200 Pro, Tecan, Austria).

2.9 *In vivo* antitumor assay

All animal procedures were performed in accordance with the Guidelines for Care and Use of Laboratory Animals of Chongqing Medical University and experiments were approved by the Animal Ethics Committee of Chongqing Medical University (China). To assess the anticancer effect of CTAC@MSN-HSA *in vivo*, breast cancer model was established by the subcutaneous injection of 1×10^6 4T1 cancer cells into nude mice (4–6 weeks old). Then the tumor-bearing mice were randomly separated into three groups ($n = 3$ per group) and subjected to intratumoral injection of saline, 2 μg mL^{-1} CTAC@MSNs, 2 μg mL^{-1} CTAC@MSNs-HSA, respectively (20 mg kg^{-1}). The therapy was repeated every 3 days within 21

days. The tumor size were also measured and calculated with the formula: the volume = (tumor length) × (tumor width)^2/2. TUNEL staining were used to analyse the toxicity of samples to tumor tissues.

2.10 Statistical analysis

Data were described as the mean ± standard deviation (SD), and statistical analysis was performed using a one-way analysis of variance (ANOVA). Statistical significance was set as *$p < 0.05$, and significant difference was set at **$p < 0.01$ and ***$p < 0.001$.

3. Results and discussion

3.1 Characterization of NPs

CTAC@MSNs were prepared through a hydrothermal method with CTAC as the structure-directing agent.[24] Different from other systems which use MSNs as drug nanocarriers, fabrication process above eliminated the need to remove the template through prolonged ethanol reflux or calcination.[10] Polydopamine (PDA) coatings are commonly used in drug delivery and their adhesive properties make them useful as substrates for anchoring biomolecules.[26] Thus, CTAC@MSNs wrapped with PDA layer are combined with HSA, which enables nanomaterials active tumor targeting ability via receptor-mediated transcytosis. Folic acid (FA) was used to block excessive sites of PDA surfaces.

TEM images are shown in Fig. 1A and S1A,† 100 particles were measured to calculate the average size of nanomaterials. MSNs and CTAC@MSNs exhibit highly uniform and spherical morphology with mean diameters of 48.5 ± 6.4 nm and 51.4 ± 4.9 nm, respectively. The morphology of CTAC@MSNs with PDA layer remains in spherical shape and uniform particle size (52.3 ± 5.0 nm). Compared with CTAC@MSNs (+PDA), CTAC@MSNs-HSA show larger particle size (59.2 ± 5.2 nm) due to the

combination with HSA and FA. The dynamic light scattering study reveals that the average hydrodynamic diameter of MSNs, CTAC@MSNs, CTAC@MSNs (+PDA) and CTAC@MSNs-HSA are 121.5 ± 4.2 nm, 111.4 ± 9.4 nm, 206.1 ± 17.4 nm and 251.4 ± 17.7 nm respectively with the polydispersity index (PDI) below 0.5 (Fig. S2, S3 and Table S1†), indicating the NPs possess relatively narrow size distribution and well dispersibility. The desirable sizes of these nanoparticles provided them with passive tumor-targeting ability via enhanced permeability and retention effect, making them ideal candidates for nanodrug therapy.

Unlike MSNs which have negative ζ potential, CTAC@MSNs show higher ζ potential due to the presence of CTAC (Fig. 1B and Table S1†). The ζ potential of CTAC@MSNs (+PDA) and CTAC@MSNs-HSA are less than −30 mV (−40.2 ± 3.10 mV and −39.5 ± 1.66 mV, respectively), indicating the stability of these nanoparticles in aqueous solution (Fig. S1B†).[19] The FTIR spectra of nanoparticles are shown in Fig. 1C and S1C.† The absorption peaks appear at 1102, 807 and 468 cm^{-1} are assigned to the Si–O–Si asymmetric stretching, Si–O–Si symmetric stretching and Si–O bending, respectively. The presence of CTAC in CTAC@MSNs and CTAC@MSNs-HSA is confirmed by the characteristic C–H stretching vibration at 2926 and 2855 cm^{-1}, while the absorption peaks of the amide I band (C=O stretching), amide II band and amide III band are observed between 1656–1392 cm^{-1}, indicating the successful combination of HSA and FA. The thermogravimetric analysis (TGA) is applied to determine the content of CTAC in MSNs (Fig. S1D†). According to the weight loss ratio, the loading amount of CTAC in CTAC@MSNs is calculated to be 11.3%.

3.2 In vitro cytotoxicity

An ideal nanocarrier should possess low toxicity and good biocompatibility. Thus, we evaluate the toxicity of MSNs against cancer cell. MCF-7 cells were incubated with various concentrations of MSNs for 24 h and 48 h. Fig. S4A† demonstrates that the cell viabilities remain over 85% even when incubated with 200 μg mL^{-1} MSNs for 48 h. In addition, similar results were obtained when MCF-7/ADR cells were treated with MSNs (Fig. S4B†), suggesting low toxicity and good biocompatibility of MSNs.

To investigate the antitumor activity of NPs, MCF-7 cells were incubated with various concentrations of CTAC@MSNs and CTAC@MSNs-HSA (containing 0.7 to 22.4 μg mL^{-1} CTAC). As shown in Fig. 2A, both CTAC@MSNs and CTAC@MSNs-HSA exhibit remarkable cytotoxicity against MCF-7 in a concentration-dependent manner. It is noteworthy that CTAC@MSNs-HSA have lower cytotoxicity than CTAC@MSNs after incubated with MCF-7 for 24 h. The half-maximum inhibitory concentration values (IC$_{50}$) of CTAC@MSNs and CTAC@MSNs-HSA are 6.06 μg mL^{-1} and 9.74 μg mL^{-1}, respectively. However, after incubating for 48 h, CTAC@MSNs-HSA show higher cytotoxicity, with the IC$_{50}$ of CTAC@MSNs and CTA@MSNs-HSA at 3.51 μg mL^{-1} and 2.85 μg mL^{-1}, respectively (Table S3†). This prolonged cytotoxicity is likely attributed to the presence of HSA, which enables the active tumor-targeting capability via
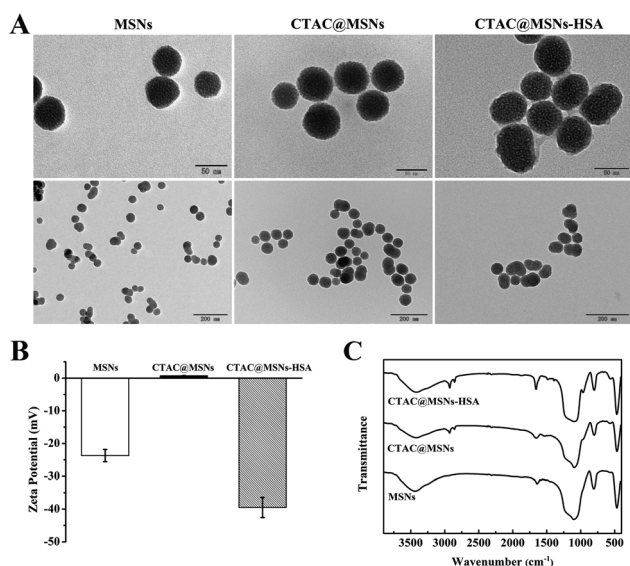

Fig. 1 (A) TEM images, (B) ζ potential and (C) FTIR spectra of MSNs, CTAC@MSNs and CTAC@MSNs-HSA NPs.
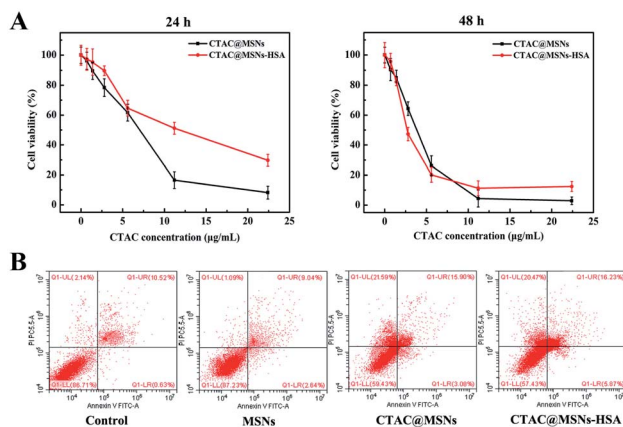
Fig. 2 (A) Cytotoxicity of NPs against MCF-7 cells after treated for 24 h and 48 h. (B) Flow cytogram images representing the necrosis and apoptosis of MCF-7 treated with MSNs, CTAC@MSNs and CTAC@MSNs-HSA solution (1 µg mL^{-1} of CTAC) for 48 h.

gp60, SPARC (secreted protein, acidic and rich in cysteine) receptor-mediated transcytosis and sustained release of CTAC from CTAC@MSNs-HSA.[23,27] CTAC@MSNs (+PDA) also show significant cytotoxicity against MCF-7 cells (Fig. S5†). As seen in Fig. S6,† the cytotoxicity of CTAC@MSNs-HSA decreases with the pretreatment of HSA, which suggests that the presence of HSA assists the cellular uptake for CTAC@MSNs-HSA. However, the cell viability of the group with pretreatment of FA did not decrease significantly. It is mainly because FA bind to PDA through the amino group, which is also the site where FA bind to FA receptor that is overexpressed in cancer cells.[26,28] Thus, FA which is a small molecule was used to cap the redundant binding sites of PDA surface rather than as a target molecule.

Cationic surfactant has been reported as a chemosensitizer for overcoming the MDR in cancer treatment and it did not possess obvious cytotoxicity for MDR cancer cells.[10] As for drug-resistant MCF-7/ADR cells, both CTAC@MSNs and CTAC@MSNs-HSA exhibit notable cytotoxicity, depending on the administration time and concentration of nanomaterials. The IC$_{50}$ (48 h) of CTAC@MSNs and CTAC@MSNs-HSA are 7.43 µg mL^{-1} and 10.38 µg mL^{-1}, which are far less than the IC$_{50}$ (21.3 µg mL^{-1}) of DOX against MCF-7/ADR cells (Fig. S7 and S8†). Moreover, the tumoricidal abilities of nanoparticles above are determined with 4T1 and C6 cells (Fig. S7†) and the corresponding IC$_{50}$ values are shown in Tables S2 and S3.† These results suggest that the antitumor activity of CTAC-loaded MSNs is remarkable to other kinds of cancer cells as well and could overcome the MDR of cancer cells *in vitro*.

The studies on mechanism of CTAC-mediated cell death are conducted by flow cytometry and apoptosis staining. As presented in Fig. 2B, MSNs have little cytotoxicity to cancer cells, which hardly cause any necrosis or apoptosis. Nevertheless, CTAC@MSNs and CTAC@MSNs-HSA simultaneously induce obvious apoptosis and necrosis of MCF-7 cells after 48 h of incubation. The effect of CTAC@MSNs-HSA on cancer cells is more related with necrosis than with apoptosis. The cell apoptosis is further assessed by Hoechst staining. After staining

with Hoechst 33258, the nuclei of normal cancer cells are blue, while the nuclei of apoptotic cells are dense and hyperchromatic with some whitish colour. According to Fig. S9,† CTAC@MSNs and CTAC@MSNs-HSA administrations increase the proportion of apoptotic cells. There is a distinct reduction in the number of cancer cells treated with CTAC@MSNs-HSA, which is possibly a result of significant cell death caused by necrosis. On the other hand, the destruction of cell membrane structure caused by cell necrosis or apoptosis leads to the release of enzymes in the cytoplasm into the culture medium.[29] Thus, we investigate the amount of LDH release in the cancer cells (Fig. S10†). Strikingly, cells treated with CTAC@MSNs shows increased LDH release compared with the untreated cells, indicating that the cells had undergone necrosis and apoptosis. Therefore, these results demonstrate that CTAC@MSNs-HSA lead to the necrosis and apoptosis of cancer cells.

The cytotoxicity of CTAC@MSNs, CTAC@MSNs (+PDA) and CATC@MSNs-HSA against MCF-10A cells was also studied in order to investigate the possible side effects of nanomaterials on normal cells. CTAC@MSNs and CTAC@MSNs (+PDA) have the higher toxicity against MCF-10A, while CTAC@MSNs-HSA has the lowest toxicity (Fig. S11†). Because the presence of HSA on CTAC@MSNs-HSA, nanoparticles are mainly taken up by cells *via* gp60 and SPARC receptor-mediated transcytosis. However, due to the few gp60 and SPARC receptors on the surfaces of normal cells, less CTAC@MSNs-HSA can enter normal cells, which makes it to be of the lowest toxicity on normal cells. As expected, CTAC@MSNs-HSA effectively target cancer cells and has reduced side effects on normal cells.

3.3 Cellular uptake and subcellular localization of NPs

The cellular uptake of nanoparticles is observed using TRITC labeled CTAC@MSNs with the lysosome stained by LysoTracker Green and mitochondrion stained by MitoLite Blue. Red fluorescence is observed after 2 h administration, indicating that the materials can enter cancer cells efficiently within 2 h of incubation and most of it are distributed in the lysosome (Fig. 3A). In general, many nanomaterials enter cells and are distributed in lysosomes. However, CTAC@MSNs are found to distribute in the mitochondria after 6 h incubation (Fig. 3B). It mainly because the materials enter cells through endocytosis at the early stage of cellular uptake, thus most of it accumulates in the lysosomes. With the prolonged incubation time, positively charged CTAC of materials let nanoparticles target to the mitochondria. Therefore, some of nanomaterials are observed in the mitochondria of cancer cells after 6 h administration.

3.4 Mitochondrial membrane potential and ATP level

CTAB has been reported as a mitochondrial inhibitor.[10,30] Based on the result that CTAC@MSNs are distributed in mitochondria, we make further investigation on the influence of CTAC@MSNs on mitochondria. JC-1 is used to measure the mitochondrial membrane potential $\Delta\Psi_m$ (MMP), which is the parameter that reflects mitochondrial function. The decrease of MMP can be detected through measuring the transformation
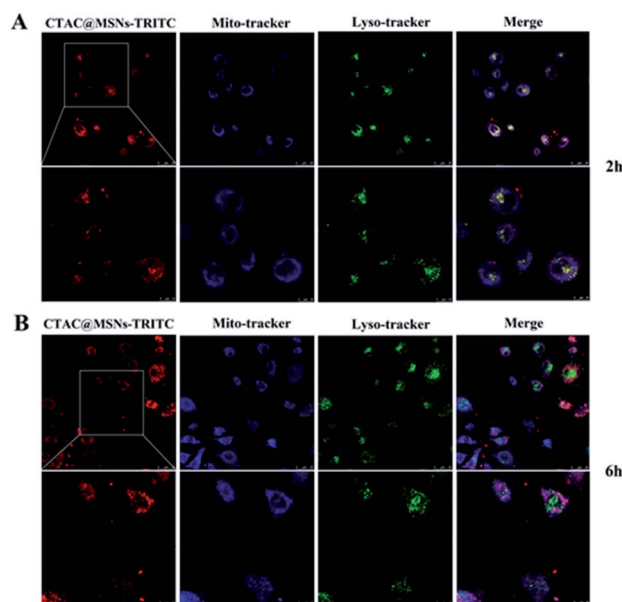
Fig. 3 CLSM images of MCF-7 cells after (A) 2 h and (B) 6 h incubation with CTAC@MSNs-TRITC (2 μg mL^{-1} of CTAC).

from red fluorescence to green fluorescence of JC-1. Red/green fluorescence ratios are significantly lower in cells treated with CTAC@MSNs than in control cells (Fig. 4A and S12†), indicating the mitochondrial membrane potential depolarization which has been hypothesized as a sign of early apoptosis in cells.[14] Thus, the decreased $\Delta\Psi_m$ confirms that the damage of mitochondria is involved with the CTAC-mediated cancer cell death.

The decrease of intracellular ATP level is usually considered as a sign of impaired mitochondria function and is often accompanied with the decrease of MMP in apoptotic cells at the same time. We further measure the intracellular ATP levels in
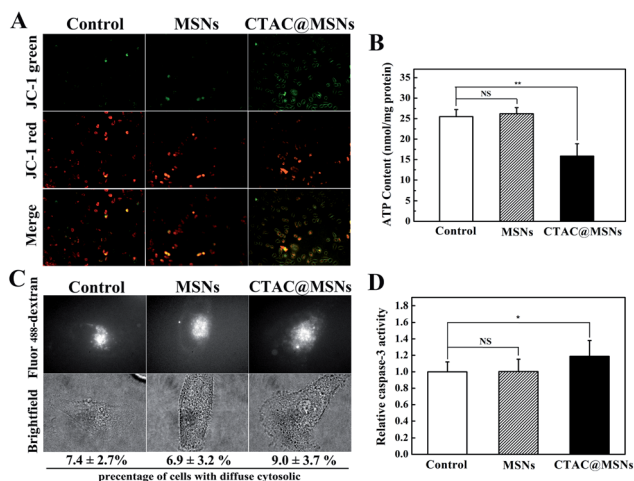

Fig. 4 The effects of MSNs, CTAC@MSNs on (A) MMP and (B) the intracellular ATP levels in MCF-7 cells treated with NPs for 24 h. (C) Imaging of LMP and (D) relative caspase-3 activities of untreated cells (control), CTAC@MSNs treated cells. NS: not significant, *$p < 0.05$, **$p < 0.01$, ***$p < 0.001$, compared with the untreated cells (control).

MCF-7 cells after nanoparticle administration. As shown in Fig. 4B, the ATP level decreased after treatment with CTAC@MSNs. This suggests that CTAC can reduce the MMP and intracellular ATP level, which further disturbs mitochondrial functions and causes mitochondrial damage. This effect is mainly due to the negative MMP (~-220 mV) which enables CTAC to greatly target the mitochondria. Similarly, a lipophilic cation, TPP is also widely applied as the mitochondria-targeting moiety.[5] Therefore, the lipophilic cation surfactant CTAC could actively target to mitochondria and further impair the mitochondrial function.

3.5 Visualization of LMP, caspase-3 activity level

The necrosis and apoptosis of cells are possibly related to the lysosomal membrane permeabilization (LMP), which releases cathepsins into the cytosol from lysosome and up-regulates active caspase-3 that plays a vital role in the execution-phase of cell apoptosis.[31,32] As described in a previous report, the fluorescent dextran changes from lysosomal punctate pattern to cytosolic diffused staining upon the increasing of LMP, which could be used to visualize the LMP by fluorescence microscope. As presented in Fig. 4C, the punctate lysosomal patterns are observed in most cells after administration. Thus, it seems that CTAC@MSNs have little impact on LMP. Moreover, compared with the control group, CTAC@MSNs induce a slight increase of caspase-3 activity after incubating with MCF-7 cells for 24 h (Fig. 4D). These observations suggest that the necrosis or apoptosis pathways caused by CTAC are mainly related to mitochondria instead of lysosomes.

3.6 *In vivo* antitumor efficacy

The antitumor effects of CTAC@MSNs and CTAC@MSNs-HSA are estimated with 4T1 tumor-bearing nude mice as a model. The nude mice received *in situ* injections of saline, CTAC@MSNs and CTAC@MSNs-HSA solution respectively, repeating every 3 days for seven consecutive cycles. The mice body weight and the tumor size were recorded every 3 days within 21 days. At the end of the treatment, the tumor tissues were dissected and stained with TUNEL method. According to Fig. 5A and B, the CTAC@MSNs group shows a slight inhibitory effect on tumor growth compared with the control group. Notably, the group treated with CTAC@MSNs-HSA exhibits an enhanced therapeutic effect. The greater therapeutic efficiency of CTAC@MSNs-HSA is mainly attributed to the presence of HSA, which increase the cell uptake of nanomaterials and improve their biocompatibility, thus provide the prolonged cytotoxicity of nanomaterials against cancer cells. Fig. 5C shows that the amount of apoptosis cells (TUNEL-positive) increased upon administration of CTAC@MSNs-HSA, which is consistent with the *in vitro* results.

The body weight of mice, served as an indicator of physiological side effects, were tracked throughout the experiment (Fig. 5D). The weight of animals administrated with CTAC@MSNs-HSA have no significant change compared with the control group. However, there is a little drop in mice weight treated with CTAC@MSNs. This indicates that the combination
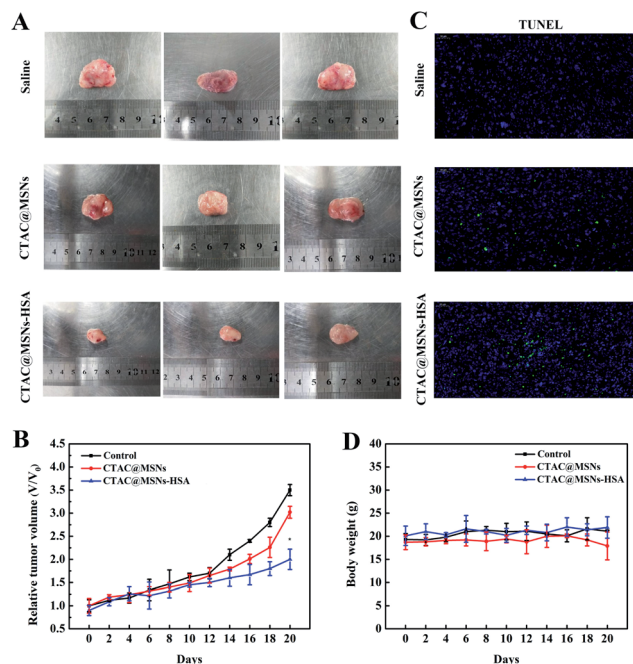
Fig. 5 (A) Images of tumors after different treatments. (B) Tumor growth curves. (C) TUNEL staining analysis of 4T1 tumor sections and (D) body weight of mice with different treatments. *$p < 0.05$, **$p < 0.01$, ***$p < 0.001$, compared with the saline treated group.

with HSA could increase the biocompatibility and reduce side effects of nanoparticles.

4. Conclusion

In this study, we develop a mitochondrion-targeting mesoporous silica nanoparticle for anticancer therapy. CTAC, as structure-directing agent, is retained in MSNs. Then, CTAC@MSNs are wrapped with PDA and combined with HSA. Due to the desirable size of nanoparticles and the presence of HSA, CTAC@MSNs-HSA can be delivered into cancer cells in a short period of time. Positively charged CTAC could target the mitochondria and further cause the dysfunction of mitochondria. As a result, CTAC@MSNs-HSA led to the necrosis and apoptosis of MCF-7 cells and showed significant antitumor activity. CTAC@MSNs-HSA not only exhibits high tumoricidal efficacy against MCF-7 cells, but also exhibits notable cytotoxicity to MCF-7/ADR, 4T1 and C6 cells. In the *in vivo* studies, this delivery system exhibits efficient inhibition of tumor growth. Overall, our experiment has shown the potential of CTAC@MSNs-HSA as a novel mitochondrion-targeting agent for anticancer therapy.

Conflicts of interest

The author(s) declare that they have no competing interests.

Acknowledgements

References

1 P. E. Porporato, N. Filigheddu, J. M. Bravo-San Pedro, G. Kroemer and L. Galluzzi, *Cell Res.*, 2018, **28**, 265–280.

2 J. A. Kashatus, A. Nascimento, L. J. Myers, A. Sher, F. L. Byrne, K. L. Hoehn, C. M. Counter and D. F. Kashatus, *Mol. Cell*, 2015, **57**, 537–551.

3 X. W. Chen, C. H. Fu, Y. Q. Wang, Q. R. Wu, X. W. Meng and K. Xu, *Nanoscale*, 2018, **10**, 15677–15685.

4 D. C. Wallace, *Nat. Rev. Cancer*, 2012, **12**, 685–698.

5 S. Kim, L. Palanikumar, H. Choi, M. T. Jeena, C. Kim and J. H. Ryu, *Chem. Sci.*, 2018, **9**, 2474–2479.

6 K. Y. Ni, G. X. Lan, C. Chan, B. Quigley, K. D. Lu, T. Aung, N. N. Guo, P. La Riviere, R. R. Weichselbaum and W. B. Lin, *Nat. Commun.*, 2018, **9**, 1–12.

7 Y. Yamada and H. Harashima, *Adv. Drug Delivery Rev.*, 2008, **60**, 1439–1462.

8 V. Weissig, S. M. Cheng and G. G. M. D'Souza, *Mitochondrion*, 2004, **3**, 229–244.

9 S. E. Weinberg and N. S. Chandel, *Nat. Chem. Biol.*, 2015, **11**, 9–15.

10 Q. J. He, Y. Gao, L. X. Zhang, Z. W. Zhang, F. Gao, X. F. Ji, Y. P. Li and J. L. Shi, *Biomaterials*, 2011, **32**, 7711–7720.

11 W. Zhang, Y. A. Shi, Y. Z. Chen, J. A. Ye, X. Y. Sha and X. L. Fang, *Biomaterials*, 2011, **32**, 2894–2906.

12 Q. J. He, X. Z. Cui, F. M. Cui, L. M. Guo and J. L. Shi, *Microporous Mesoporous Mater.*, 2009, **117**, 609–616.

13 R. L. Grant, C. Yao, D. Gabaldon and D. Acosta, *Toxicology*, 1992, **76**, 153–176.

14 E. Ito, K. W. Yip, D. Katz, S. B. Fonseca, D. W. Hedley, S. Chow, G. W. Xu, T. E. Wood, C. Bastianutto, A. D. Schimmer, S. O. Kelley and F. F. Liu, *Mol. Pharmacol.*, 2009, **76**, 969–983.

15 D. Q. Chen, G. Q. Zhang, R. M. Li, M. R. Guan, X. Y. Wang, T. J. Zou, Y. Zhang, C. R. Wang, C. Y. Shu, H. Hong and L. J. Wan, *J. Am. Chem. Soc.*, 2018, **140**, 7373–7376.

16 Y. H. Cheng, H. Cheng, C. X. Jiang, X. F. Qiu, K. K. Wang, W. Huan, A. Yuan, J. H. Wu and Y. Q. Hu, *Nat. Commun.*, 2015, **6**, 1–8.

17 S. Shen, C. L. Zhu, D. Huo, M. X. Yang, J. J. Xue and Y. N. Xia, *Angew. Chem., Int. Ed.*, 2017, **56**, 8801–8804.

18 S. P. Wang, J. M. Zhang, Y. T. Wang and M. W. Chen, *J. Nanomed. Nanotechnol.*, 2016, **12**, 411–420.

19 L. M. Wang, Q. Sun, X. Wang, T. Wen, J. J. Yin, P. Y. Wang, R. Bai, X. Q. Zhang, L. H. Zhang, A. H. Lu and C. Y. Chen, *J. Am. Chem. Soc.*, 2015, **137**, 1947–1955.

20 L. Yu, Y. Chen, M. Wu, X. Cai, H. Yao, L. Zhang, H. Chen and J. Shi, *J. Am. Chem. Soc.*, 2016, **138**, 9881–9894.

21 N. Menon and D. T. Leong, *ACS Appl. Mater. Interfaces*, 2016, **8**, 2416–2422.

22 P. Horcajada, T. Chalati, C. Serre, B. Gillet, C. Sebrie, T. Baati, J. F. Eubank, D. Heurtaux, P. Clayette, C. Kreuz, J. S. Chang, Y. K. Hwang, V. Marsaud, P. N. Bories, L. Cynober, S. Gil, G. Ferey, P. Couvreur and R. Gref, *Nat. Mater.*, 2010, **9**, 172–178.

23 Z. H. Sheng, D. H. Hu, M. B. Zheng, P. F. Zhao, H. L. Liu, D. Y. Gao, P. Gong, G. H. Gao, P. F. Zhang, Y. F. Ma and L. T. Cai, *ACS Nano*, 2014, **8**, 12310–12322.

24 L. M. Pan, Q. J. He, J. N. Liu, Y. Chen, M. Ma, L. L. Zhang and J. L. Shi, *J. Am. Chem. Soc.*, 2012, **134**, 5722–5725.

25 W. Y. Huang, J. N. Lin, J. T. Hsieh, S. C. Chou, C. H. Lai, E. J. Yun, U. G. Lo, R. C. Pong, J. H. Lin and Y. H. Lin, *ACS Appl. Mater. Interfaces*, 2016, **8**, 30722–30734.

26 M. E. Lynge, R. van der Westen, A. Postma and B. Stadler, *Nanoscale*, 2011, **3**, 4916–4928.

27 J. Xu, J. J. Wang, J. C. Luft, S. M. Tian, G. Owens, A. A. Pandya, P. Bergund, P. Pohlhaus, B. W. Maynor, J. Smith, B. Hubby, M. E. Napier and J. M. DeSimone, *J. Am. Chem. Soc.*, 2012, **134**, 8774–8777.

28 H. Lee, S. M. Dellatore, W. M. Miller and P. B. Messersmith, *Science*, 2007, **318**, 426–430.

29 J. Nylandsted, M. Gyrd-Hansen, A. Danielewicz, N. Fehrenbacher, U. Lademann, M. Hoyer-Hansen, E. Weber, G. Multhoff, M. Rohde and M. Jaattela, *J. Exp. Med.*, 2004, **200**, 425–435.

30 S. W. Kim, M. Kim, W. Y. Lee and T. Hyeon, *J. Am. Chem. Soc.*, 2002, **124**, 7642–7643.

31 P. Boya and G. Kroemer, *Oncogene*, 2008, **27**, 6434–6451.

32 Z. Wen, Y. Long, L. Yang, J. Hu, N. Huang, Y. Cheng, L. Zhao and H. Zheng, *RSC Adv.*, 2016, **6**, 105814–105820.